# Selective Fluorescence Detection of Metronidazole in Traditional Dairy Products Using Green-Synthesized Carbon Quantum Dots Enhanced by Experimental Design and Machine Learning

**Sepideh Gharehyakheh**
Islamic Azad University
**changiz karami**
changiz.karami@gmail.com
Islamic Azad University
**Sadaf Pirouzi**
Department of Convergent Sciences & Technologies

**Research Article**

**Keywords:** Carbon quantum dots, Rosa Canina synthesis, Metronidazole detection, Fluorescence sensor, Experimental design, Machine learning, Antibiotic monitoring

**Posted Date:** July 8th, 2026

**DOI:** https://doi.org/10.21203/rs.3.rs-10186809/v1



**Additional Declarations:** No competing interests reported.

# Abstract

CQDs were synthetized by a green hydrothermal method starting from Rosa Canina as natural carbon source in the present contribution. Fluorescence spectroscopy, FTIR, SEM, EDX and elemental mapping were employed to examine the structural and optical properties of CQDs in this research. The in situ synthesis resulted in a nanocomposite that combines good fluorescence emission properties, which permits sensitive detection of metronidazole (MNZ) through fluorescence quenching. Using a Design of Experiments (DoE), sensor parameters were optimised and demonstrated linear detection range of 5.0–400.0 μM, limit of detection = 2.24 μM, limit of quantification 7.39 μM with good repeatability RSD = 3.38%, n = 12 and reproducibility (RSD = 3.47%). The use of machine learning to enhance predictive accuracy and provided interpretation of data. The practical applicability is verified through the successful identification of MNZ in real dairy products with low co-extraction and acceptably recovery.


# 1. Introduction

Food safety and quality are essential for protecting public health, growth and development. In addition to general hygiene regulations during production, processing, and storage food must be contaminant free—especially from hazardous materials such as antibiotic residues. Over the past few decades, extensive use of antibiotics in agriculture and livestock farming has increased significantly for prevention and treatment of diseases. The excessive and improper use of these substances have led to the accumulation of antimicrobial residues in the food supplies, which makes us face some important concerns about potential harms on public health [1, 2].

The frequent use of antibiotics in livestock production, although helpful in fighting many bacterial infections, has played an important role in the emergence of antibiotic-resistant bacterial strains [3]. This increasing resistance represents a major threat to public health by making treatment more complex, raising healthcare expenses and hindering global health security. Moreover, the residual effect of antibiotics in food derived from animals (meat, milk and eggs) has been reported to be linked to allergic reactions and a number of other health effects in humans. Therefore, the need for strict monitoring and regulation of antibiotic use in agri-food systems is critical to address these risks to protect human as well as environmental health [3].

Antimicrobial resistance, on the one hand, directly affects the intestinal bacteria of humans and animals, endangering their health and disrupting their work. On the other hand, this intestinal microbiota controls many physiological processes, such important physiological processes such as digestion, nutrients absorption, vitamin biosynthesis and immune modulation., and when this microbial balance is disrupted by antibiotic use, digestive disorders such as diarrhea and inflammation occur [4].

Abstract Metronidazole is a broad-spectrum antimicrobial drug frequently used in the treatment of adult and pediatric infections due to anaerobic bacteria and protozoa in both human and veterinary medicine. Its use in animal husbandry has established itself as a standard practice, especially for therapy and prophylaxis. Nevertheless, inappropriate use of metronidazole in food producing animals generates a

potential risk of residues being present in edible animal products (e.g. meat and milk). The consumption of these contaminated foods may present a serious risk for consumers, who can develop allergic responses (hypersensitivity), induction of the gut microbiota and appearance of metronidazole-resistant microbial strains. Such risks form the basis of strong justification about rigorous epidemiological surveillance and regulatory oversight in antibiotic use and animal agriculture to assure food safety and protect human health [5, 6]. Metronidazole is an antibiotic commonly used to treat parasitic infections in both humans and animals. There are several health risks associated with the presence of metronidazole in food such as developing gastrointestinal symptoms, neuropathy, and the potential of cancer. Ingesting antibiotics promotes the development of antibiotic-resistant infections which poses an even bigger risk to health. Because of the potential of these health risks, there should be more quick and accurate tests to determine whether or not food contains metronidazole. These tests would ensure the safety of the food supply and the control of antibiotic use [7, 8].

Considering that different methods have been previously reported for measuring the amount of metronidazole, these methods had some drawbacks (such as high-performance liquid chromatography (HPLC), electrochemical assays, UV-Vis spectroscopy) regarding their accuracy and reliability. Which can be explained by the expensiveness of the measuring devices, the complicated and difficult preparation, as well as the matrix interference causing the decrease in sensitivity. On the other hand, the measurement of the decrease in sensitivity may have deviated from the standard detection limit. Now, considering this limitation, with the upcoming research, they are looking for a new method with less limitation and more accuracy [9–12]. Due to its high sensitivity and very short response time—which make it superior to other methods—fluorescence spectroscopy is becoming increasingly important. As a result, the development of fluorescent materials and compounds is increasingly becoming the focus of research. Another reason for the importance of this method is the use of compounds (nanostructures) that have been able to increase the sensitivity and accuracy of fluorescence spectroscopy many times over [13].

Driven by the principles of green chemistry, researchers are increasingly turning to bio-based waste to synthesize carbon quantum dots (CQDs) that are both affordable and environmentally benign [14].In this work, we utilized mold as a novel carbon source to fabricate high-performance fluorescent probes. This strategy serves a dual purpose: it transforms biological waste into a high-value material while significantly boosting the sensor’s optical performance to enable ultra-sensitive metronidazole detection. By merging sustainability with analytical rigor, this approach highlights a highly promising, cost-effective pathway for developing advanced, eco-friendly detection systems [15, 16].

To address the need for safer analytical methods, we developed a green synthesis route for carbon quantum dots (CQDs) using Rosa canina, a naturally abundant plant source. These eco-friendly CQDs serve as the foundation for a new fluorescence sensor designed to detect metronidazole in traditional dairy products. Rather than relying on trial and error, we optimized the sensor’s performance using Design of Experiments (DoE) and integrated machine learning algorithms for advanced predictive

modeling. This combination is fully in line with the principles of green chemistry and has been validated for the successful measurement of MNZ in real samples.

## 2. Experimental

## 2.1. Reagents and materials

The mountain rose plant was collected from the Kermanshah mountains [17]. Then it was dried in the shade and after crushing, it was poured into distilled water and heated to boiling point. After 1 hour, the resulting extract was filtered. The obtained solution should be concentrated to be prepared for the next steps. Other materials including antibiotics and NaOH, and HCl were purchased from Merck. Also, double distilled water was used to prepare the solutions.

## 2.2 Synthesis of Carbon Quantum Dots (CQDs)

Carbon quantum dots are synthesized from the extract of the Rosa Canina plant. 50 ml of the extract is poured into a Teflon autoclave and placed in it at a temperature of 200°C for 24 h. After cooling, the solution is filtered and quantum dots are synthesized.

## 2.3 Characterization Techniques

A set of different techniques were used to evaluate the optical structure and morphology of the synthesized carbon quantum dots. A PerkinElmer LS 45 spectrofluorometric was used to measure fluorescence emission optical properties and a Thermos Avatar model was used to identify surface functional groups by Fourier transform infrared spectroscopy (FTIR). A scanning electron microscope (FE-SEM, TESCAN MIRA III) at 15 kV, along with EDX, elemental mapping, and line scan analyses, were used to examine the morphology and elemental abundance and percentage.

## 2.4 Experimental Design and Optimization

A central composite design (CCD) was used to optimize the CQDs sensor in Design-Expert software (version 11.1.1.0). The study included three independent variables: pH (4.0–10.0), reaction time (0.5–5.0 min), and temperature (34–60°C) and consisted of a one-pot experimental design consisting of 20 runs (Table 1). The fluorescence response was modeled using a second-order polynomial equation (Eq. 1) that included linear, quadratic, and interaction terms. After statistical validation of the model via ANOVA ($p < 0.05p < 0.05p < 0.05$), three-dimensional response surface plots were studied to visualize the interactions of the parameters and establish the optimal operating conditions for the sensor.

Table 1
Experimental parameters and levels in the 20 CCD for the optimization of pH, Temp, and Time

| Factor | Name | Level | Low Level | High Level | Std. Dev. | Coding |
|---|---|---|---|---|---|---|
| A | pH | 5.50 | 3.00 | 8.00 | 0.0000 | Actual |
| B | Time | 9.50 | 4.00 | 15.00 | 0.0000 | Actual |
| C | Temp. | 45.00 | 30.00 | 60.00 | 0.0000 | Actual |

$$Y = \beta 0 + (\beta_1 \times A) + (\beta_2 \times B) + (\beta_3 \times C) + (\beta_{11} \times A_2) + (\beta_{22} \times B_2) + (\beta_{33} \times C_2) + (\beta_{12} \times AB) + (\beta_{13} \times AC) + (\beta_{23} \times BC) \quad (1)$$

In the provided equation, Y represents the predicted response, and β0 denotes the model constant. The coefficients $\beta_1$, $\beta_2$, $\beta_3$, $\beta_{11}$, $\beta_{22}$, $\beta_{33}$, $\beta_{12}$, $\beta_{13}$, and $\beta_{23}$ within the statistical model, the linear, quadratic, and interaction effects of factors A (pH), B (Temperature), and C (Time) on the response are demonstrated

Table 1

# 2.5 Fluorescence Sensing Procedure

To investigate the sensitivity of the synthesized carbon quantum dots to different concentrations of metronidazole, 30 µg of CQDs were dissolved in 3 mL of aqueous buffer solution with pH 7. Then, fluorescence emission spectra were recorded with an excitation wavelength of 420 nm and an emission intensity of 550 nm. the intensity ratio (F0/F), which is the ratio of the initial fluorescence to the fluorescence intensity after the addition of the analyte, Also, the limit of detection (LOD) was determined using the signal-to-noise ratio criterion (S/N = 3), which represents the lowest detectable concentration of metronidazole.

# 2.6 Machine Learning Analysis

To improve how well the fluorescence sensor could predict metronidazole levels, a set of supervised machine-learning models was tested using Python (v. 3.13.2) together with the Scikit-learn tools. The experimental data were fed into six different regression approaches—Support Vector Regression (SVR), Random Forest Regression (RFR), Artificial Neural Networks (ANN), k-Nearest Neighbors (KNN), Gradient Boosting Regression (GBR), and Decision Tree Regression (DTR). Each model was trained and then checked to see how well it handled the relationship between the variables. Their performance was judged using the usual statistical indicators: $R^2$ to show how much of the variation the model could explain, and RMSE and MAE to see how far the predictions drifted from the real values. After comparing all of them, the model that managed to keep the errors lowest while giving the highest $R^2$ was selected as the most reliable option for estimating metronidazole concentration.

# 2.7. Preparation of sample

To assess the practical applicability of the CQD-based sensor, raw milk was obtained from a local supermarket. Sample preparation was carefully carried out to precipitate proteins and extract the analyte effectively. 10 ml of distilled water is poured into 4 ml of raw milk, then 2 ml of 10% trichloroacetic acid is added, and the mixture is mixed by stirring and placing in an ultrasonic bath, then neutralized with sodium hydroxide, and the clear part is separated by centrifugation and stored. To determine recovery rates, milk samples were spiked with known concentrations of MNZ, processed using this exact extraction method, and analyzed under the optimized fluorescence conditions [22].

## 3. Results and discussion

# 3.1 Structural and Morphological Characterization

To evaluate the morphology and size of the synthesized carbon quantum dots (CQDs), surface imaging and elemental analyses were conducted. Figure 1A presents the surface morphology, confirming the uniformity and spherical shape of the nanoparticles. Elemental mapping analysis (Fig. 1B) was used to examine the distribution of elements on the sample surface. The results showed that the carbon element, which is shown in green, has the highest amount of about 50.9%. In addition to carbon, oxygen was also detected at about 26% and the presence of other elements including potassium, calcium, magnesium and sulfur. Their presence could be due to mineral compounds, as well as the natural origin of the plant.

Therefore, the type and amount of these elements may vary depending on the geographical origin and growing conditions of the plant used. Transmission electron microscopy (TEM) analysis provided a clearer view of the nanoparticle morphology (Fig. 2A), showing that the CQDs are nearly spherical with an average diameter of about 2 nm. In Fig. 2B, line scanning visually plots the spatial distribution of surface elements.

The variations in peak intensities along the scan line indicate a heterogeneous distribution of elements (such as carbon, oxygen, magnesium, and potassium) both on the surface and within the CQDs, an integration that can significantly influence their optical, chemical, and biological behavior.

Figure 3A basically shows the FTIR spectra for both the Rosa canina extract and the CQDs we made (R-CQDs). When you look at the curves, you can spot the usual signals for the carboxyl (− COOH) and hydroxyl (− OH) groups — the bumps around 1700 $cm^{-1}$ and 3300 $cm^{-1}$. They’re still there, which means these groups didn’t disappear during synthesis and stayed in the structure. For the fluorescence part, we checked how the CQDs behave under different excitation wavelengths, from 280 up to 350 nm. At the lower excitations (something like 280–320 nm), the emission wasn’t very sharp — more like wide, fuzzy peaks. But when the excitation went above 320 nm, the peaks suddenly looked cleaner and stronger. The nicest and clearest signal happened at 360 nm, giving a well-defined emission peak around 450 nm (Fig. 3B). It’s pretty obvious that the CQDs respond much better at that point. Finally, UV-Vis spectroscopy highlights notable optical differences between glucose-derived and Rosa canina-derived

CQDs (**Fig. S1**). Glucose-derived CQDs exhibit a broad absorption band around 200–300 nm, characteristic of π-π∗ transitions in aromatic carbon structures. In contrast, the Rosa canina-derived CQDs display a distinct peak near 350 nm, indicating the presence of surface states associated with oxygen-containing functional groups. This finding, alongside the elemental and FTIR analyses, suggests that the R-CQDs possess a higher degree of surface functionalization, likely facilitated by phytochemicals from the plant extract, which enhances their surface chemistry and optical absorption.

Figure 1

Figure 2

Figure 3

# 3.2. Statistical analysis

To systematically evaluate and optimize the fluorescence quenching response ($F_0/F$) of the CQD-based sensor for metronidazole detection, Response Surface Methodology (RSM) utilizing a Central Composite Design (CCD) was employed. A total of 16 experimental runs were conducted to investigate the interactive effects of pH (A), temperature (B), and reaction time © on the sensor's performance. The detailed experimental conditions and their corresponding $F_0/F$ responses, which ranged from 1.09 to 1.16, are outlined in Table 2. This range confirms that the selected parameters measurably influenced the fluorescence quenching behavior. Among the linear, two-factor interaction (2FI), and quadratic models evaluated, the quadratic model yielded the best statistical fit. As detailed in Table 3, this model achieved a high adjusted $R^2$ of 0.9919 and a predicted $R^2$ of 0.9653, demonstrating a robust correlation between the experimental and predicted responses with minimal overfitting. The high statistical significance of the model was confirmed by a sequential p-valuep of < 0.0001. The model also passed the lack-of-fit test, since the p-value was extremely small (around 0.0005), which basically shows that the model fits the data well enough to be trusted for prediction. After going through the analysis, the final quadratic equation—written using the coded variables—is presented below.

Table 2
Experiment runs and responses for optimizing parameters evaluation

| Run | Factor 1 | Factor 2 | Factor 3 | Response 1 |
|---|---|---|---|---|
| | A: pH | C: Time | B: Temp | $F_0/F$ |
| 1 | 5.5 | 9.5 | 70 | 1.16 |
| 2 | 3 | 4 | 60 | 1.11 |
| 3 | 5.5 | 0.5 | 45 | 1.1 |
| 4 | 5.5 | 9.5 | 45 | 1.16 |
| 5 | 5.5 | 9.5 | 45 | 1.16 |
| 6 | 5.5 | 9.5 | 45 | 1.16 |
| 7 | 5.5 | 9.5 | 45 | 1.16 |
| 8 | 5.5 | 19 | 45 | 1.12 |
| 9 | 8 | 4 | 30 | 1.12 |
| 10 | 8 | 4 | 60 | 1.12 |
| 11 | 3 | 15 | 60 | 1.13 |
| 12 | 5.5 | 9.5 | 20 | 1.16 |
| 13 | 10 | 9.5 | 45 | 1.09 |
| 14 | 2 | 9.5 | 45 | 1.12 |
| 15 | 3 | 15 | 30 | 1.13 |
| 16 | 5.5 | 9.5 | 45 | 1.16 |
| 17 | 5.5 | 9.5 | 45 | 1.16 |
| 18 | 8 | 15 | 60 | 1.13 |
| 19 | 3 | 4 | 30 | 1.11 |
| 20 | 8 | 15 | 30 | 1.13 |

Table 3
Model summary statistic.

| Source | Sequential p-value | Lack of Fit p-value | Adjusted $R^2$ | Predicted $R^2$ | |
|---|---|---|---|---|---|
| Linear | 0.7551 | | -0.1047 | -0.4540 | |
| 2FI | 0.9953 | | -0.3527 | -1.2849 | |
| **Quadratic** | **< 0.0001** | | **0.9919** | **0.9653** | **Suggested** |
| Cubic | | | 1.0000 | | Aliased |

$Y = 1.16 + 0.0012A + 0.0075B - 0.0000C - 0.0212A^2 - 0.0175B^2 - 0.0003C^2 - 0.0025AB + 0.0000AC + 0000BC$

In this model, the positive coefficients basically show that the variables are working together to boost the fluorescence signal, while the negative ones point to effects that push in the opposite direction or weaken the response. What stands out the most is how strongly temperature and pH affect the system—both on their own and when they interact with each other. They clearly play a major role in shaping how the sensor behaves. Overall, the statistical results make it pretty clear that the quadratic model is solid enough to rely on for predicting trends and figuring out the best operating conditions to get the strongest sensor response.

Table 2

Table 3

# 3.3. ANOVA

An Analysis of Variance (ANOVA) was conducted to assess the statistical validity of the quadratic model used to predict the fluorescence quenching response ($F_0/F$) (Table 4). The model shows a very strong fit overall. The F-value is quite large (around 260.94), and the p-value is well below 0.0001, which basically means the chance of this fit happening randomly is extremely small—less than a hundredth of a percent. When looking at the individual terms, reaction time (B) and the pH–time interaction (AB) clearly stand out. Their p-values are extremely low (< 0.0001 for B and about 0.0073 for AB), so they play a major role in shaping the response. The quadratic terms for pH ($A^2$) and time ($B^2$) were also highly significant ($p < 0.0001$), which confirms that both variables have a strong nonlinear effect on the sensing behavior. On the other hand, temperature (C), its interaction terms (AC and BC), and even its quadratic term ($C^2$) didn't show meaningful effects under the tested conditions ($p > 0.05$). They were still kept in the model, though, just to maintain the proper hierarchy and avoid breaking the structure of the regression equation. While the lack-of-fit p-valuep\ (0.0005) indicated some significant deviation, the extremely low residual error (Mean Square Residual = $4.45\times10^{-6}$) renders this variance acceptable within typical analytical limits. Overall, the statistical evaluation demonstrates the model's robust predictive capability and confirms the

efficacy of the CCD-RSM approach for system optimization. The final quadratic equation, formulated using actual experimental values, is given as:

Table 4
ANOVA for response surface quadratic model for $F_0/F$

| Source | Sum of Squares | df | Mean Square | F-value | p-value | |
|---|---|---|---|---|---|---|
| **Model** | 0.0105 | 9 | 0.0012 | 260.94 | < 0.0001 | significant |
| A-pH | 0.0000 | 1 | 0.0000 | 3.86 | 0.0779 | |
| B-Time | 0.0008 | 1 | 0.0008 | 172.62 | < 0.0001 | |
| C-Temp. | 1.735E-18 | 1 | 1.735E-18 | 3.898E-13 | 1.0000 | |
| AB | 0.0000 | 1 | 0.0000 | 11.24 | 0.0073 | |
| AC | 1.735E-18 | 1 | 1.735E-18 | 3.898E-13 | 1.0000 | |
| BC | 1.735E-18 | 1 | 1.735E-18 | 3.898E-13 | 1.0000 | |
| $A^2$ | 0.0058 | 1 | 0.0058 | 1302.56 | < 0.0001 | |
| $B^2$ | 0.0044 | 1 | 0.0044 | 997.08 | < 0.0001 | |
| $C^2$ | 1.310E-06 | 1 | 1.310E-06 | 0.2944 | 0.5993 | |
| **Residual** | 0.0000 | 10 | 4.450E-06 | | | |
| Lack of Fit | 0.0000 | 5 | 8.900E-06 | | | |
| Pure Error | 0.0000 | 5 | 0.0000 | | | |
| **Cor Total** | 0.0105 | 19 | | | | |

$$Y = + 0.9830 + (0.0395 \times A) + (0.0131 \times B) - (0.0001 \times C) - (0.0033 \times A^2) - (0.0005 \times B^2) + (1.3567 \times C^2) - (0.0001 \times AB) + (0.0000 \times AC) + (0.0000 \times BC) \quad (2)$$

This equation illustrates how each factor contributes to the fluorescence intensity and allows for effective prediction and optimization of conditions for metronidazole analysis.

Table 4

## 3.4. 3D response surface plots

Three-dimensional response surface plots were generated from the quadratic model to assess the interactive and individual effects of pH (A), time (B), and temperature (C) on the fluorescence response ($F_0/F$). Each plot compares two variables while keeping the third one fixed at its midpoint. In **Fig. S2A**, the interaction between pH and time is pretty obvious — the surface bends noticeably, and the contours look more elliptical, which suggests that these two factors reinforce each other. There's a clear sweet

spot where the quenching reaches its maximum. In **Fig. S2B**, which compares pH with temperature, the interaction between the two is pretty minimal. The contours are almost straight, so it's clear that pH is the main factor driving the response. Temperature only causes a slight drop in the signal, and that mostly happens when the pH is already on the higher side. And then in **Fig. S2C**, you can see how time and temperature behave together. It gives a general idea of how these two variables shape the response when pH is kept fixed at its center level. The relatively flat surface confirms minimal interaction, with the response increasing over time but remaining largely independent of temperature across the tested range. Overall, the 3D models confirm that pH and reaction time are the critical parameters governing fluorescence quenching, demonstrating the utility of RSM in identifying optimal experimental conditions.

# 3.5. Accuracy of the Model

As detailed in Table 5, the quadratic model governing the fluorescence quenching response ($F_0/F$) exhibits exceptional statistical reliability. The model yields a high coefficient of determination ($R^2$ = 0.9958), explaining 99.58% of the response variability. The adjusted $R^2$ value (0.9919) lines up really well with the predicted $R^2$ (0.9653). The difference between them is tiny (less than 0.03) which basically shows that the model predicts new data almost as well as it fits the existing data, without signs of overfitting. The experiments were also very consistent; the standard deviation was extremely low (about 0.0021), and the coefficient of variation was only 0.1859%, which is almost negligible. Another strong point is the adequate precision value, which came out to 45.2147. Since anything above 4 is considered acceptable, this number is way beyond the minimum and shows that the signal-to-noise ratio is excellent. Putting all of these together, the statistical indicators make it pretty clear that the model is solid, reliable, and well-suited for fine-tuning the conditions needed to accurately detect metronidazole using carbon quantum dots.

Table 5

Standard deviation and $R^2$ of the response.

| **Std. Dev.** | **0.0021** | **$R^2$** | **0.9958** |
|---|---|---|---|
| **Mean** | 1.13 | **Adjusted $R^2$** | 0.9919 |
| **C.V. %** | 0.1859 | **Predicted $R^2$** | 0.9653 |
| | | **Adeq Precision** | 45.2147 |

Table 5

# 3.6 Model Diagnostics and Assumptions Verification

We checked several diagnostic plots (**Fig. S3A–D**) to make sure our quadratic model works properly and follows the main rules of regression. The residuals in **Fig. S3A** are spread randomly, which means their variance is stable. Fig. S3B shows that the residuals follow a normal pattern, so there are no major outliers. In **Fig. S3C**, the predicted values line up closely with the actual measurements, which shows that the model is doing a good job overall. There are only small differences at the extreme ends, and

that's pretty normal in experimental work. Fig. S3D doesn't show any pattern over time, meaning the experiment stayed consistent and there weren't any systematic errors creeping in. Putting everything together, these results make it clear that the model satisfies the main assumptions and can be trusted for predicting and optimizing amoxicillin removal.

**Figure 8**

## 3.7. Machine Learning Model Evaluation for Metronidazole Prediction

To compare the predictive performance of machine learning models in the detection of metronidazole, three common algorithms—linear regression, Random Forest, and Support Vector Regression (SVR)—were evaluated using the most important statistical metrics: the coefficient of determination ($R^2$), the root mean square error (RMSE), and the mean absolute error (MAE). The three-dimensional comparison ($R^2$–RMSE–MAE space) shown in Fig. 4A clearly illustrates the differences in performance among the models. Among these, the Random Forest model performs best and is located in the optimal region, as it exhibits the highest $R^2$ value (approximately 0.96) as well as the lowest RMSE and MAE values. These results indicate this model's high ability to detect nonlinear relationships in the data and provide accurate and reliable predictions. In contrast, the linear regression and SVR models are in a range with poorer performance, characterized by negative $R^2$ values and higher errors. Their limited predictive capability suggests that their underlying assumptions—strict linearity in Linear Regression and fixed kernel structure in SVR—are insufficient to model the complexity and variability present in the data. Figure 4B backs up the earlier results by showing how the predicted values compare with the actual measurements for each model. The Random Forest points (the green ones) fall almost right on top of the diagonal line, which means the predictions barely deviate from the real data — basically a very tight match. In contrast, the Linear Regression (red) and SVR (blue) points drift away from that line, and you can clearly see the gap, which tells you their predictions aren't as reliable. Taken together, the results make it pretty obvious why ensemble methods like Random Forest tend to perform better when the dataset is complex and involves several variables, which is often the case in analytical chemistry and sensor development. Their ability to stay stable, adapt to patterns, and still give precise outputs makes them genuinely useful for improving detection methods and pushing data-driven optimization in real applications.

Figure 4

## 3.8. Method Selectivity

To check how selective, the sensing system really is, a wide range of antibiotics and structurally similar compounds were tested — things like amoxicillin, azithromycin, ceftriaxone, cefixime, ciprofloxacin, clamoxin, cotrimoxazole, doxycycline, levofloxacin, metronidazole, ofloxacin, rickettsia, tetracim, tetracycline, and a few others. Each one was added to the sensing medium at the same concentration, and the fluorescence response was measured and then normalized against the blank. For most of these

compounds, the normalized fluorescence stayed very close to 1, which basically means they didn't interact with the sensing material in any meaningful way. This shows that the system isn't easily affected by random or nonspecific interference. Metronidazole stood out from the rest — its signal jumped quite a bit, reaching around 1.23, which makes it pretty clear that it behaves differently from the other compounds. Doxycycline, on the other hand, barely changed anything. Its value was roughly 1.002, which is so small that it doesn't really have any meaningful effect. Altogether, these results make it pretty clear that the sensor reacts very specifically to metronidazole, while staying steady and unaffected when other antibiotics with similar structures or functions are present. This level of selectivity makes the system well-suited for detecting metronidazole in more complex aqueous samples, which is promising for real-world analytical and environmental applications (**Fig. S4**).

# 3.9. Calibration and Detection of Metronidazole

The CQDs synthesized from *Rosa canina* exhibited strong intrinsic fluorescence, which was noticeably enhanced upon interaction with metronidazole (MNZ). Under optimized sensing conditions, the fluorescence intensity increased progressively with rising MNZ concentrations, forming the basis for their use as a sensitive and environmentally friendly fluorescence sensor. To assess the analytical performance of the system, MNZ solutions ranging from 5.0 to 400.0 μM were introduced into the sensing medium, and the fluorescence intensity ratio ($F_0/F$) was plotted against MNZ concentration. As shown in Fig. 5A, the sensor shows a clear linear trend across the tested range, and the points fit the line really well. The high $R^2$ value backs this up and shows that the measurements were consistent and precise. For the detection limits, the LOD and LOQ were calculated from the blank's standard deviation and the slope of the calibration curve. They came out to about 2.24 μM and 7.39 μM (Fig. 5B), which are quite low and point to the strong sensitivity of the sensing system. The fluorescence enhancement seems to come from the way MNZ molecules interact with the functional groups on the surface of the CQDs. This interaction likely shifts the local electronic environment a bit and makes radiative recombination more favorable, which explains the stronger signal. When you put this together with the clear linear behavior, the low detection limits, and the consistent enhancement mechanism, it shows that the CQDs-based sensor can reliably and accurately quantify metronidazole in aqueous samples.

Figure 5

# 3.10. Interference Study for Metronidazole Detection

To further assess the specificity of the sensing platform, potential interference studies were performed by introducing common coexisting compounds into the metronidazole solution. The fluorescence intensity of 250 μM metronidazole alone was compared with its intensity in the presence of 500 μM of various interfering species, including $Ca^{2+}$, $K^+$, $Na^+$, lactose, casein, vitamin C, riboflavin, triglycerides, lactic acid, and tetracycline. The results showed that the fluorescence signal remained essentially unchanged upon addition of these substances, indicating that none of them produced a meaningful effect on the detection of metronidazole. This stability in fluorescence response demonstrates the high specificity of the CQDs-based sensor, even in the presence of compounds commonly found in complex

sample matrices such as food or biological fluids. Accordingly, the developed sensing system is capable of reliably quantifying metronidazole without significant interference from typical coexisting components (**Fig.S5**).

# 3.11. Application

To evaluate how well the CQDs-based fluorescent nanoprobe performs in real situations, traditionally sourced dairy products were chosen as representative samples, since they are directly relevant to food safety monitoring. The samples were first homogenized and then diluted tenfold in a pH 5 buffer, which helped reduce matrix complexity while still keeping the conditions close to what would be expected in an actual analytical setting. Under the optimized sensing conditions, different concentrations of metronidazole (10, 150, and 300 μM) were added to the prepared dairy matrices, and the resulting fluorescence signals were measured. The concentrations were then calculated using the established calibration curve. As shown in Table 6, the method produced strong recovery values—100.5%, 101.7%, and 100.63%—across the three spiking levels. The corresponding RSD values (2.94%, 2.54%, and 1.12%) also indicate that the measurements were precise and highly repeatable. These results show that the CQDs-based sensor maintains its accuracy and reliability even when dealing with complex food matrices. Because of this, the fluorescence method provides a fast, sensitive, and environmentally friendly way to quantify metronidazole in traditional dairy products, making it suitable for routine food safety assessments.

Table 6
Determination of metronidazole concentration in real samples. By fluorescence method (n = 5)

| sample | Spiked value metronidazole (μM) | Found value<br><br>by the sensor metronidazole<br><br>(μM) | RSD% | Recovery (%) |
|---|---|---|---|---|
| 1 | 10 | 10.5 ± 0.27 | 2.94 | 100.5 |
| 2 | 150 | 151.60 ± 3.85 | 2.54 | 101.7 |
| 3 | 300 | 352.20 ± 3.96 | 1.12 | 100.63 |
| Relative standard error: RSD | | | | |

Table 7 compares this system with other sensors previously reported for metronidazole detection, summarizing their linear ranges, detection limits, and real-sample applications. Sodium-based carbon quantum dots showed a linear range of 20–100 μM with an LOD of 62.5 nM in water samples. A molecularly imprinted polymer sensor offered a linear range of 5.0–60.0 μM and an LOD of 1.28 μM in real matrices. Nitrogen-doped fluorescent carbon dots demonstrated higher sensitivity, with a linear range of 0.5–22 μM and an LOD of 0.22 μM in urine samples. The CQDs sensor developed in this study provides a competitive linear range of 5.0–350.0 μM and an LOD of 2.24 μM, and it was successfully applied to serum samples. Although its LOD is higher than some of the more sensitive systems, the

much broader linear range and its proven performance in complex biological matrices highlight its strong potential for clinical monitoring of metronidazole [18–20].

Table 7
Comparison of the performances of various sensors for detection of metronidazole

| Probe | Linear range | LOD | Antibiotics | Real sample | [Ref] |
|---|---|---|---|---|---|
| sodium based-carbon quantum dots | 20–100 µM | 62.5 nM | metronidazole | water samples | [18] |
| molecular imprint polymer for metronidazole extraction–detection | 5.0–60.0 µM | 1.28 µM | metronidazole | real samples | [19] |
| nitrogen-doped fluorescent carbon dots | 0.5–22 µM | 0.22 µM | metronidazole | urine samples | [20] |
| CQDs of mod | 5.0-350.0 µM | 2.24 µM | metronidazole | serum samples | This work |

Table 6

Table 7

# 4. Conclusions

In this study, a green, cost-effective, and highly sensitive fluorescence sensor was successfully developed using carbon quantum dots (CQDs) synthesized from Rosa canina via a simple hydrothermal method. Comprehensive characterization using techniques such as TEM, FTIR, SEM, EDX, line-scan analysis, elemental mapping, and fluorescence spectroscopy confirmed that the CQDs possessed the structural and optical features needed for sensing. The nanoprobe showed a strong and stable fluorescence signal that responded selectively to metronidazole (MNZ), mainly through a quenching-based mechanism. From an analytical standpoint, the sensor performed very well: it offered a broad linear detection range (5.0–350.0 µM), a low detection limit of 2.24 µM, and showed high repeatability and reproducibility. The Design of Experiments (DoE) optimization further improved the system's efficiency. Machine-learning models were also added to the workflow, mostly to see whether they could improve the predictions and give a better sense of how the sensor behaves under different conditions. When these models were tested, they helped sharpen the overall predictive performance and made the behavior of the system a bit easier to interpret. In the selectivity experiments, it turned out that the usual interfering substances—things like metal ions, proteins, sugars, or even antibiotics with somewhat similar structures—didn't really change the fluorescence signal in any meaningful way. The response stayed almost the same, which shows that the CQDs-based platform is genuinely selective. The method also performed very well in real dairy samples. The recovery values were high, and the measurements stayed consistent, which means the system works reliably even when the sample matrix is messy and

full of natural components. It didn’t need complicated pretreatment either, which is a practical advantage. Altogether, the CQDs-based nanoprobe developed in this study seems to offer a dependable and environmentally friendly option for monitoring antibiotics. Its strong sensitivity and selectivity, along with its good performance in real samples, suggest that it could be used routinely for food-safety checks and possibly even broader public-health monitoring, especially in traditional or artisanal dairy products.

# Declarations


### Acknowledgements

The authors gratefully acknowledge the support and laboratory facilities provided by the Islamic Azad University of Kermanshah.


### Author contributions

**Sepideh Gharehyakheh**: Conducted the experimental work, synthesized the carbon quantum dots, and collected fluorescence data.

**Changiz Karami**: Assisted in data analysis, machine learning modeling, and optimization experiments.

**Sadaf Pirouzi:** Contributed to study design, manuscript preparation, and data interpretation.

All authors reviewed and approved the final version of the manuscript. Sepideh Gharehyakheh is the corresponding author.

### Competing interests

The authors declare that they have no known competing financial interests or personal relationships that could have appeared to influence the work reported in this paper.

### Data availability

All data generated or analyzed during this study are available from the corresponding author upon reasonable request.

### Ethics declarations

All milk samples used in this study were commercially available and purchased from local dairy sources in Kermanshah. The samples were used solely for analytical purposes, and no human or animal subjects were directly involved. Therefore, ethical approval and informed consent were not required for this study.

### Consent to participate / Consent for publication

Not applicable.

**Funding**

This research did not receive any specific grant from funding agencies in the public, commercial, or not-for-profit sectors.

# References

1. Shahid, A., Ali, M. A., Muzammil, S., Aslam, B., Shahid, M., Saqalein, M., Akash, M. S. H., Almatroudi, A., Allemailem, K. S., & Khurshid, M. (2021). Antibiotic residues in food chains; impact on the environment and human health: a review. *Applied Ecology & Environmental Research* 19.
2. Kyuchukova, R. (2020). Antibiotic residues and human health hazard-review. *Bulgarian Journal of Agricultural Science* 26.
3. Van Boeckel, T. P., Brower, C., Gilbert, M., Grenfell, B. T., Levin, S. A., Robinson, T. P., Teillant, A., & Laxminarayan, R. (2015). Global trends in antimicrobial use in food animals, Proceedings of the National Academy of Sciences 112 5649–5654.
4. Francino, M. (2016). Antibiotics and the human gut microbiome: dysbioses and accumulation of resistances. *Frontiers in Microbiology*, *6*, 164577.
5. Ljubojević Pelić, D., Radosavljević, V., Pelić, M., Živkov Baloš, M., Puvača, N., Jug-Dujaković, J., & Gavrilović, A. (2024). Antibiotic Residues in Cultured Fish: Implications for Food Safety and Regulatory Concerns. *Fishes*, *9*, 484.
6. Baynes, R. E., Dedonder, K., Kissell, L., Mzyk, D., Marmulak, T., Smith, G., Tell, L., Gehring, R., Davis, J., & Riviere, J. E. (2016). Health concerns and management of select veterinary drug residues. *Food and Chemical Toxicology*, *88*, 112–122.
7. Baynes, R. E., Dedonder, K., Kissell, L., Mzyk, D., Marmulak, T., Smith, G., Tell, L., Gehring, R., Davis, J., & Riviere, J. E. (2016). Health concerns and management of select veterinary drug residues. *Food and Chemical Toxicology*, *88*, 112–122.
8. Kyuchukova, R. (2020). Antibiotic residues and human health hazard-review. *Bulgarian Journal of Agricultural Science* 26.
9. Karami, C., & Taher, M. A. (2018). Colorimetric Sensor of Cobalt Ions in Aqueous Solution Using Gold Nanoparticles Modified with Glycyrrhizic Acid. *Plasmonics*, *13*. https://doi.org/10.1007/s11468-017-0635-9
10. Deymehkar, E., Taher, M. A., Karami, C., & Arman, A. (2018). Synthesis of SPR Nanosensor using Gold Nanoparticles and its Application to Copper (II) Determination, Silicon 10 https://doi.org/10.1007/s12633-017-9608-z
11. Karami, C., Mehr, S. Y., Deymehkar, E., & Taher, M. A. (2018). Naked Eye Detection of $Cr^{3+}$and $Co^{2+}$Ions by Gold Nanoparticle Modified with Azomethine. *Plasmonics*, *13*. https://doi.org/10.1007/s11468-017-0541-1

12. Karami, C., Taher, M. A., & Shahlaei, M. (2020). A simple method for determination of mercury (II) ions by PNBS-doped carbon dots as a fluorescent probe. *Journal of Materials Science: Materials in Electronics*, *31*, 5975–5983.
13. Jain, P. K., Huang, X., El-Sayed, I. H., & El-Sayed, M. A. (2008). Noble metals on the nanoscale: optical and photothermal properties and some applications in imaging, sensing, biology, and medicine. *Accounts of Chemical Research*, *41*, 1578–1586.
14. Kneipp, J., Kneipp, H., Wittig, B., & Kneipp, K. (2010). Novel optical nanosensors for probing and imaging live cells. *Nanomedicine: Nanotechnology Biology and Medicine*, *6*, 214–226.
15. Hou, J., Li, H., Wang, L., Zhang, P., Zhou, T., Ding, H., & Ding, L. (2016). Rapid microwave-assisted synthesis of molecularly imprinted polymers on carbon quantum dots for fluorescent sensing of tetracycline in milk. *Talanta*, *146*, 34–40.
16. Liu, G., Chen, Z., Jiang, X., Feng, D. Q., Zhao, J., Fan, D., & Wang, W. (2016). In-situ hydrothermal synthesis of molecularly imprinted polymers coated carbon dots for fluorescent detection of bisphenol A. *Sensors and Actuators B: Chemical*, *228*, 302–307.
17. Arslan, E. S., Akyol, A., Örücü, Ö. K., & Sarıkaya, A. G. (2020). Distribution of rose hip (Rosa canina L.) under current and future climate conditions. *Regional Environmental Change*, *20*, 107.
18. Alvarenga, L. M., dos Reis Feliciano, C., Alvarenga, B. G., de Paula, H. M. C., Coelho, Y. L., da Silva, L. H. M., Gorup, L. F., Santos, M. G., & Virtuoso, L. S. (2023). Preparation of a composite sensor based on a fluorescent and magnetic molecular imprint polymer for metronidazole extraction–detection. *Journal of Molecular Liquids*, *390*, 123027.
19. Xia, Z., & Li, Q. (2022). Application of Metronidazole detection by antibiotic ampicillin sodium based-carbon quantum dots. *International Journal of Environmental Analytical Chemistry*, *102*, 4178–4190.
20. Ren, G., Hou, X., Kang, Y., Zhang, R., Zhang, M., Liu, W., Li, L., Wei, S., Wang, H., & Wang, B. (2020). Efficient preparation of nitrogen-doped fluorescent carbon dots for highly sensitive detection of metronidazole and live cell imaging. *Spectrochimica Acta Part A: Molecular and Biomolecular Spectroscopy*, *234*, 118251.

# Figures

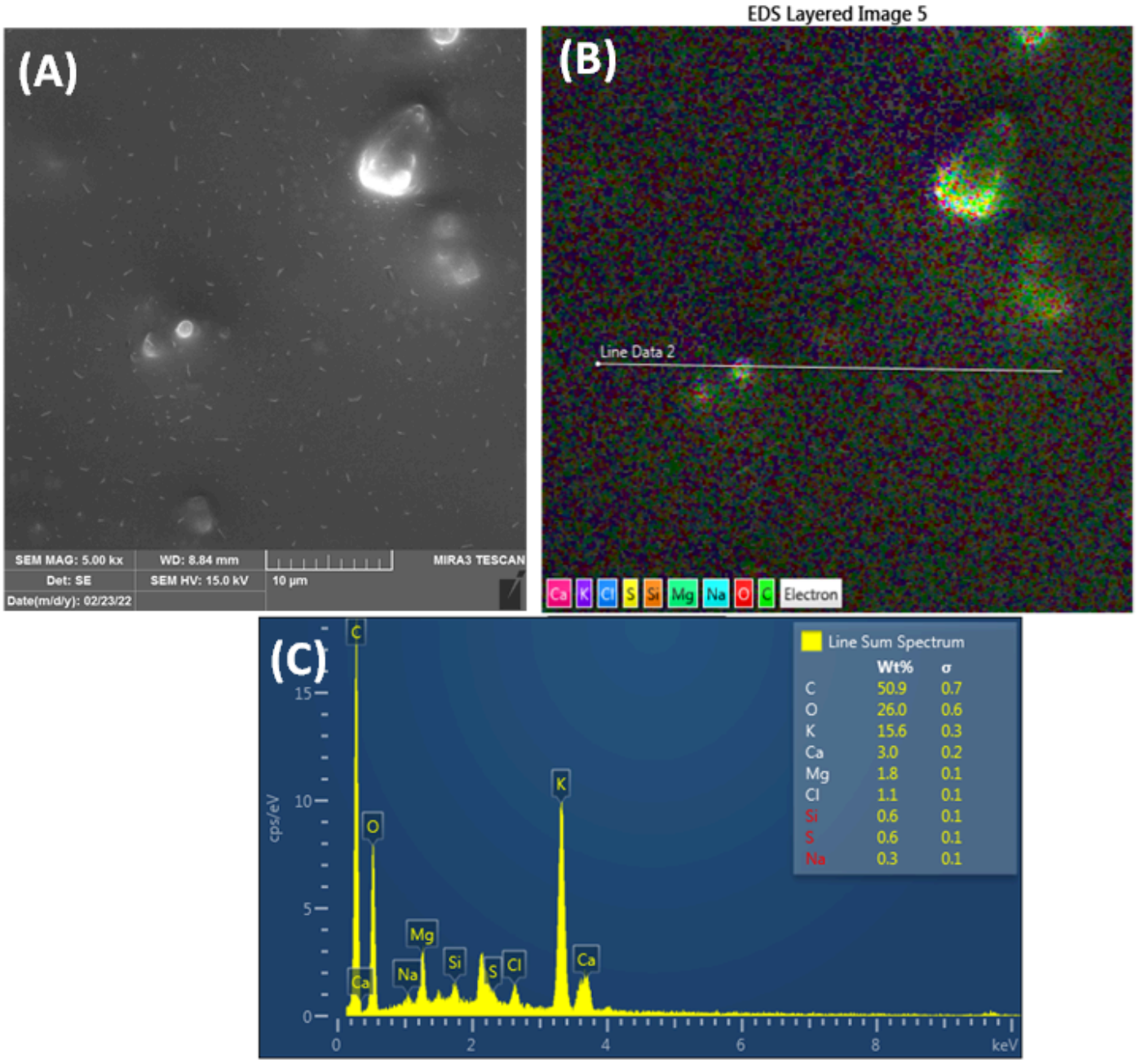


**Figure 1**

A) SEM images, mapping imaging, C) EDS of R-CQDs

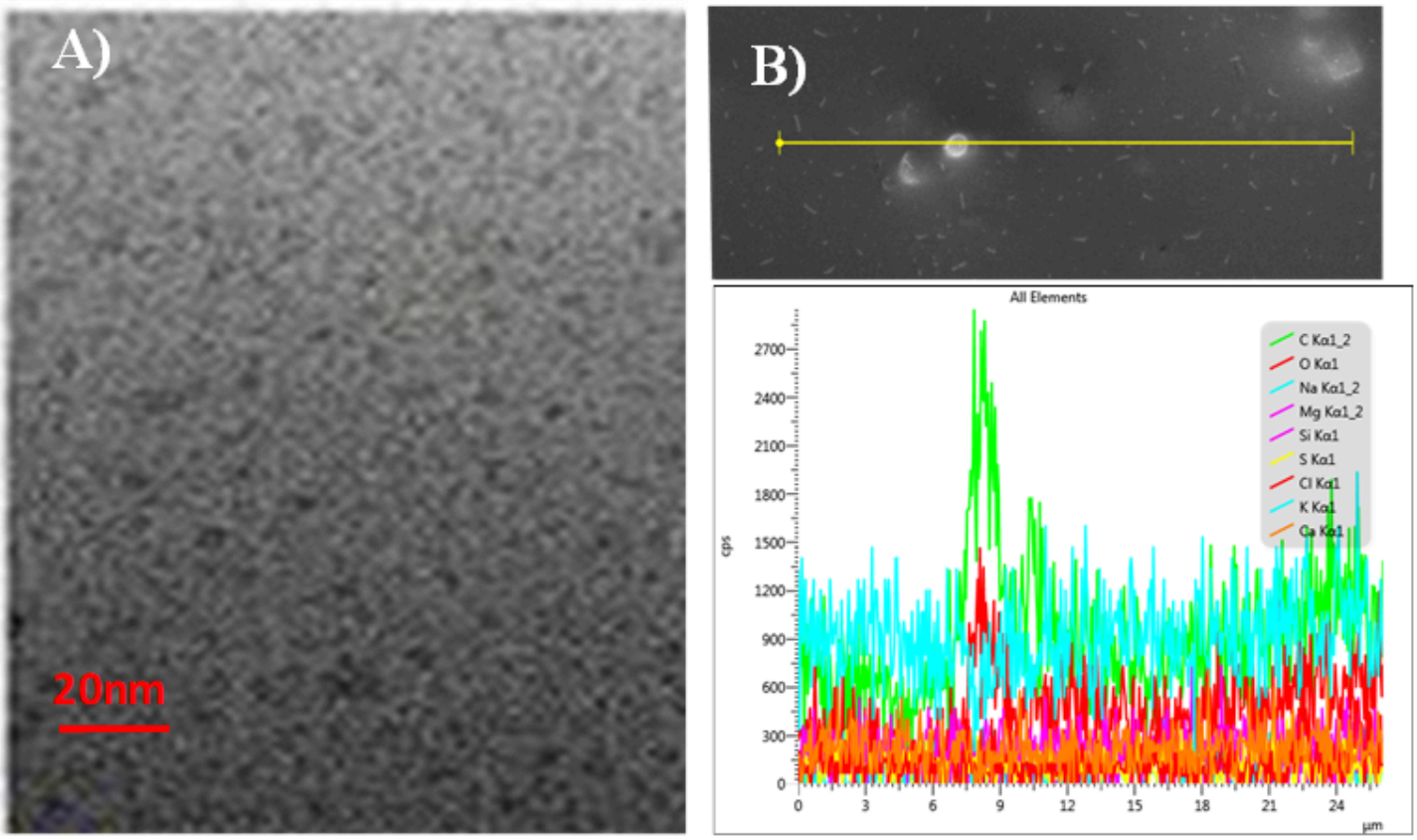


**Figure 2**

A) TEM images of R-CQDs, B) line scanning of R-CQDs

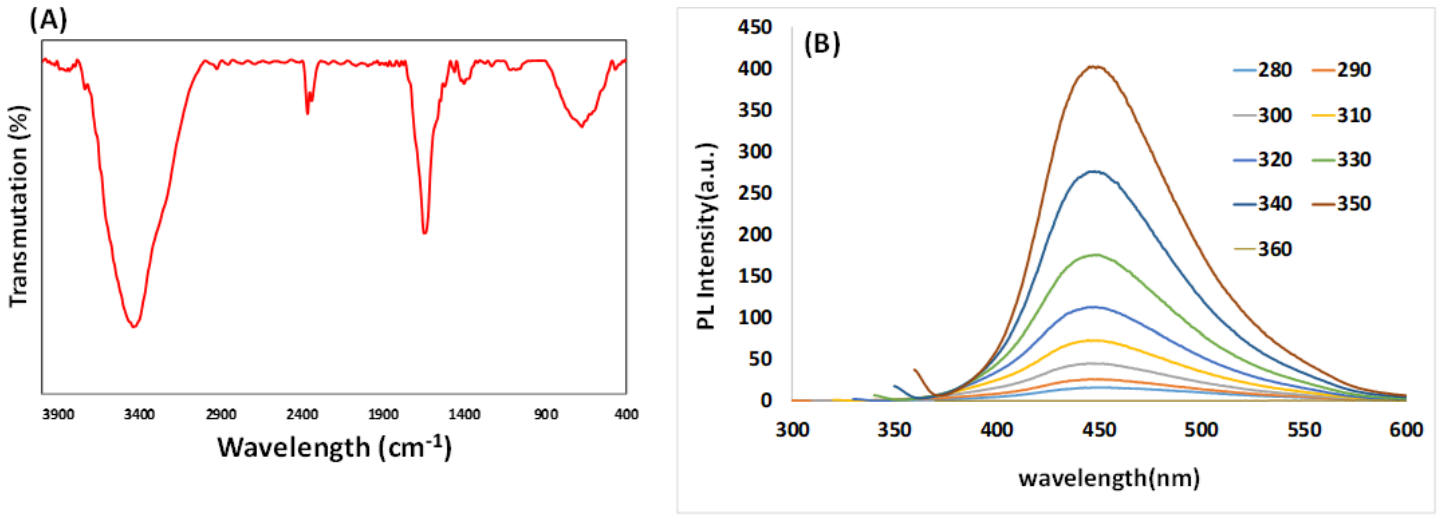


**Figure 3**

A) FTIR spectra of R-CQDs, B) Fluorescence spectrum of R-CQDs in excitation with different wavelengths from 280 nm to 350 nm

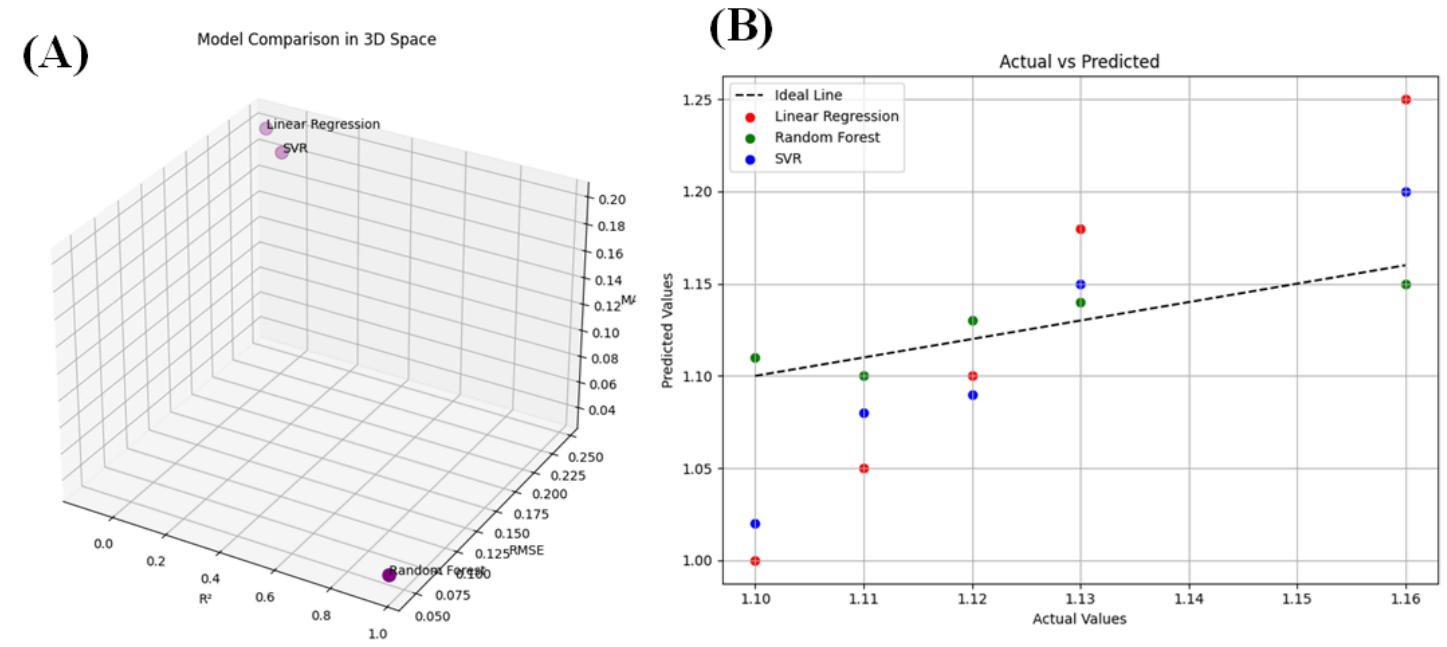


**Figure 4**

**(A)** 3D Scatter Plot of Model Performance. The plot visualizes the Mean Squared Error (MSE) and R-squared values for each model, with the z-axis representing the model indices, (B) Model Performance: Actual vs. Predicted values

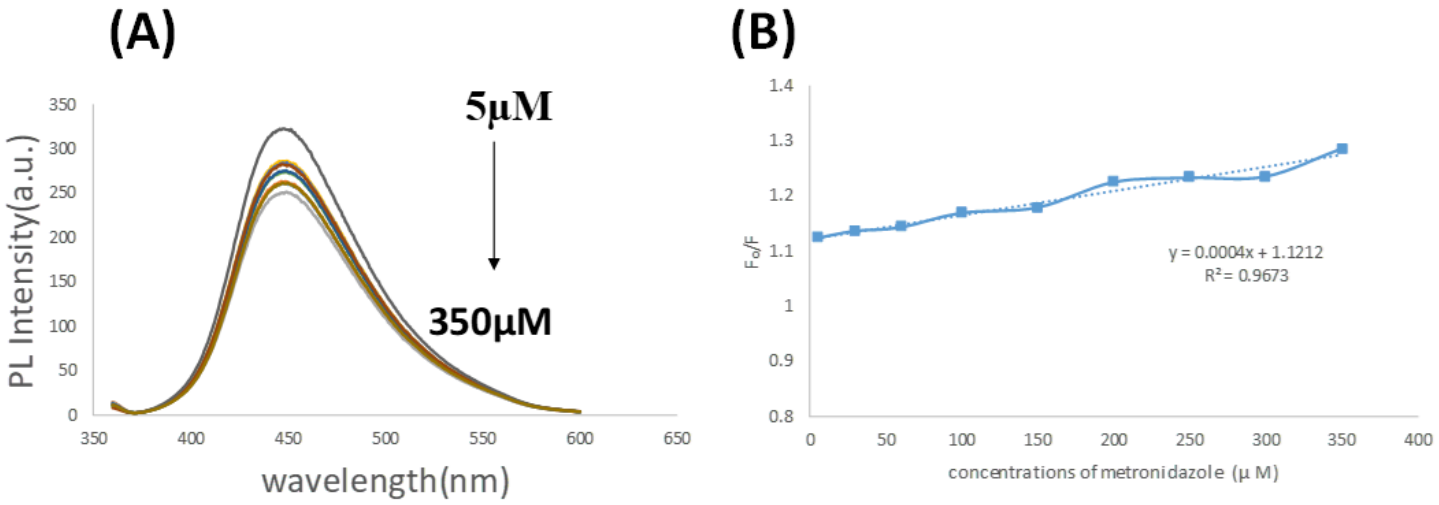


**Figure 5**

A) Change in the fluorescence intensity of the R-CQDs compound in the presence of different concentrations of metronidazole from 5.0 to 350.0 μM. B) Increasing the relative sensitivity of the detection system with different concentrations of metronidazole, 5.0 to 350.0 μM

## Supplementary Files

This is a list of supplementary files associated with this preprint. Click to download.

- SupportingInformation.docx